Environmental Health
Engineering and
Management Journal

Original Article

Optimizing the removal of methylene blue from aqueous solutions using persulfate activated with nanoscale zero valent iron (nZVI) supported by reduced expanded graphene oxide (rEGO)

Alaa Mohamad Soubh[1]* , Mohammad Ali Abdoli[1] , Lorin Ali Ahmad[2]

[1]School of Environment, College of Engineering, University of Tehran, Tehran, Iran
[2]Tartus Research Center, General Commission for Scientific Agriculture Research (GCSAR), Damascus, Syria

Abstract

Background: To remove methylene blue (MB) from aqueous solutions, nanoscale zero-valent iron (nZVI) predicated on reduced expanded graphene oxide (rEGO) was used as the activator of persulfate.

Methods: Scanning electron microscope (SEM) and energy dispersive spectroscopy (EDS) analyses were used to investigate the surface morphology and to examine the surface elemental composition. X-ray diffraction (XRD) was used to determine the chemical compositions of the synthesized compound. In this study, the effects of pH (3-9), activator dose (0.4-1.6 g L^{-1}), persulfate concentration (0.192-0.768 g L^{-1}), and reaction time (0-60 minutes) on the removal of 10 mg L^{-1} MB were studied by nZVI -reduced expanded graphene oxide/persulfate (nZVI@rEGO/PS) process.

Results: The maximum removal efficiencies of MB at optimum operational conditions (pH 3, activator dose = 1.2 g L^{-1}, persulfate concentration = 0.576 g L^{-1}, and reaction time = 20 minutes) by nZVI@rEGO/PS process was 96%. The chemical method was used to prepare expanded graphene. The volume of natural flake graphite increased about 25 times after the process. SEM image of the nZVI@rEGO showed the presence of nZVI placed on the EGO surface in chain structure with a diameter about 100 nm. The EDS analysis of the activator indicated the existence of Fe element to an amount greater than 50%.

Conclusion: According to the results, nZVI@rEGO is considered as a promising activator of persulfate.

Keywords: Persulfate, Methylene blue, Graphite, Graphene oxide, Kinetics

Citation: Soubh AM, Abdoli MA, Ahmad LA. Optimizing the removal of methylene blue from aqueous solutions using persulfate activated with nanoscale zero valent iron (nZVI) supported by reduced expanded graphene oxide (rEGO). Environmental Health Engineering and Management Journal 2021; 8(1): 15-24. doi: 10.34172/EHEM.2021.03.

*Correspondence to:
Alaa Mohamad Soubh,
Email: soubh@ut.ac.it

Introduction

The colored wastewater produced by industrial activities, such as textile industry and color production, has toxic effects on aquatic ecosystems (1). The presence of aromatic rings in the structure of azo dyes has increased the toxicity of these compounds and decreased their biodegradability (2). Dyes are among the most dangerous chemical compounds that can interfere with the process of photosynthesis in water resources. Methylene blue (MB) with molecular formula of $C_{16}H_{18}ClN_3S$ and with molar mass of 319.85 g/mol is one of the azo-cationic dyes (3,4). Its chemical structure is shown in Figure 1. It is also used in various industries, such as textile, paper paints, hair color, etc. Intense exposure to MB leads to severe damages to the human body (2,5). MB belongs to azo dyes family which contain the functional group R-N=N-R′ in their structure and constitute a very large group of all coloring agents used. Azo dyes are a triggering factor for histamine, which may exacerbate the symptoms of asthma, and cause

uterine contractions in pregnant women, resulting in miscarriage. Additionally, in combination with benzoates, they can cause hyperactivity in children. Even for non-allergic persons, they may be the cause of, for example, urticaria (6). Therefore, due to environmental problems and human health, treatment of wastewater containing these compounds has become a vital issue (5).

The activation of persulfate ($S_2O_8^{2-}$, $E° = 2.01$ V) has attracted the interest of many researchers especially in the fields associated with the removal of pollutants (7-9). Activation of persulfate (PS) leads to the generation of sulfate radical (SR, $SO_4^{•-}$, $E° = 2.5$-3.1 V). Many studies have confirmed the effectiveness of SR on degradation of refractory pollutants (10,11). Recently, many studies have indicated that zero-valent iron (ZVI) can be used as a suitable heterogeneous activator of PS (12,13). ZVI is converted to Fe^{+2} according to several mechanisms: (1) Through its interaction with hydrogen ion (H^+) (Eq. 1); (2) Interaction with PS ions (Eq. 2); (3) Interaction with
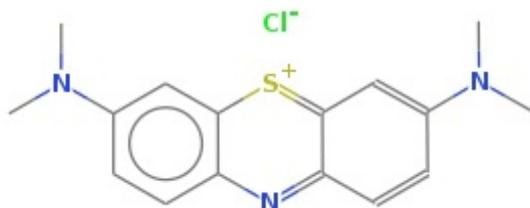
Figure 1. Chemical structure of methylene blue.

O_2 and H_2O in the aqueous solution (Eqs. 3 and 4); (4) Recovery interaction with Fe^{+3} (Eq. 5) (14-16). The Fe^{+2} ions activate PS according to Eq. (6).

$$Fe^o + 2H^+ \rightarrow Fe^{2+} + H_2 \tag{1}$$

$$Fe^o + S_2O_8^{2-} \rightarrow Fe^{2+} + 2SO_4^{2-} \tag{2}$$

$$2Fe^o + O_2 + 2H_2O \rightarrow 2Fe^{2+} + 4OH^- \tag{3}$$

$$2Fe^o + 2H_2O \rightarrow Fe^{2+} + 2OH^- + H_2 \tag{4}$$

$$2Fe^{3+} + Fe^o \rightarrow 3Fe^{2+} \tag{5}$$

$$S_2O_8^{2-} + Fe^{2+} \rightarrow SO_4^{\cdot-} + SO_4^{2-} + Fe^{3+} \tag{6}$$
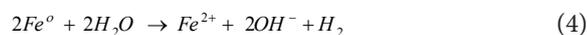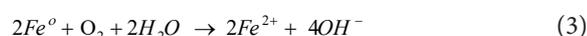
Nanoscale ZVI (nZVI) has a higher surface area leading to more efficient results of activating PS (17,18). Bare nZVI tends to be agglomerated and oxidized, which reduces its efficiency (19,20). This disadvantage of nZVI can be prevented by supporting and dispersing nanoparticles on solid materials (21), such as resin (22), kaolinite (23) , biochar (24), chitosan/silica (25), carbon (26), and graphene (27).

Graphene has a two-dimensional structure and a suitable surface area that make it a pre-eminent nanoparticle carrier (28,29). The reduction of graphene oxide (GO) improves the performance of graphene when used as a nanoparticle carrier (30). For example, reduced graphene oxide-supported nanoparticles contributed to preventing the aggregation (31). Furthermore, expanded graphene oxide (EGO) with high quality and large surface area is suitable for environmental applications (32). Composites of nZVI with reduced graphene oxide (rGO) achieved the desired results in the removal of contaminants, such as Pb(II) (33), As(III), As(V) (34), and Cd(II) (35). Ahmad et al reported nZVI-rGO as an excellent and efficient persulfate activator than unsupported nZVI for degradation of trichloroethylene (36). EGO is a graphite derivative by chemical expansion of natural flake graphite. EGO has lower mobility in the porous media compared to GO. This feature makes it an environmentally friendly material. Recently, Dong et al have suggested a chemical method for the expansion of graphite as a pretreatment step for the synthesis of EGO. The expansion of graphite layers results in the fast diffusion of oxidant between layers even at low concentrations; as a result, the oxidation process is performed at room temperature. Furthermore, EGO with high quality and high surface area is suitable for environmental applications (32).

In this study, EGO was prepared by the chemically expanded graphite. Reduced EGO (rEGO) was used as a bed for the immobilization of nZVI. The nZVI@rEGO was used as the activator of PS to remove MB from aqueous solutions. Moreover, the effects of essential factors affecting the performance of PS/nZVI@rEGO process, such as pH, nZVI@rEGO dose, PS dosage, contact time, and temperature were evaluated.

Materials and Methods
Materials
Natural flake graphite (NFG) (100-mesh) was obtained from Yantai Lushun Huitong Biotechnology (Yantai, China). $C_{16}H_{18}N_3SCl$ (≥97%), $Na_2S_2O_8$ (99%), CrO_3 (98%), $KMnO_4$ (99%), KI (99%), and NaBH4 (97%) were obtained from Loba-Chemie (Mumbai, India). $FeSO_4 \cdot 7H_2O$ (99.5%), NaOH (≥ 97.0%), HCl (37%), H_2SO_4 (98%), and H_2O_2 (30%) were purchased from Merck Company. Deionized water was used for the preparation of aqueous solutions.

Synthesis of rEGO-supported nZVI
At first, expanded graphite (EG) was papered by mixing 1g of NFG, 8.5 g of CrO_3, and 70 mL of HCl for 2 hours. In order to remove the remaining CrO_3, the prepared EG was soaked in distilled water 4 consecutive times. To complete the chemical expansion reactions, the resulted EG was submerged in 40 mL of H_2O_2 for 20 hours. Then, the EG was washed with distilled water and ethanol 4 consecutive times (32). The previous stage can be explained through the following equations: The presence of CrO_3 and HCl together leads to the production of CrO_2Cl_2 between graphite layers (Eq. 7), the penetration stage. Adding H_2O_2 to the penetrated EG leads to the hydrolysis of CrO_2Cl_2 to CrO_5 at acidic condition (Eqs. 8 and 9). The generated CrO_5 interacts with H_2O_2 and oxygen gas is released between graphite layers which leads to its expansion (Eq. 10), the expansion stage (37,38). As shown in Figure 2a, it almost doubled in size to 25 times.

$$CrO_3 + 2HCl \rightarrow CrO_2Cl_2 + H_2O \tag{7}$$

$$2CrO_2Cl_2 + 3H_2O \rightarrow H_2Cr_2O_7 + 4HCl \tag{8}$$

$$Cr_2O_7^{-2} + 2H^+ + 4H_2O \rightarrow 2CrO_5 + 5H_2O \tag{9}$$

$$2CrO_5 + 6H^+ + 7H_2O_2 \rightarrow 2Cr^{3+} + 10H_2O_2 + 7O_2 \uparrow \tag{10}$$
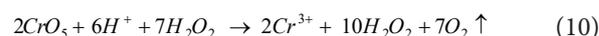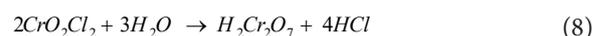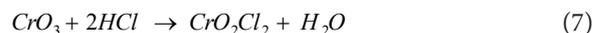
Before starting the oxidation process, the EG was soaked in H_2SO_4 to eliminate the remained internal H_2O between graphite layers for 10 minutes. Then, 2 g of $KMnO_4$ was mixed with 20 mL of H_2SO_4 in an ice bath for 30 minutes. After that, the mixture was removed from
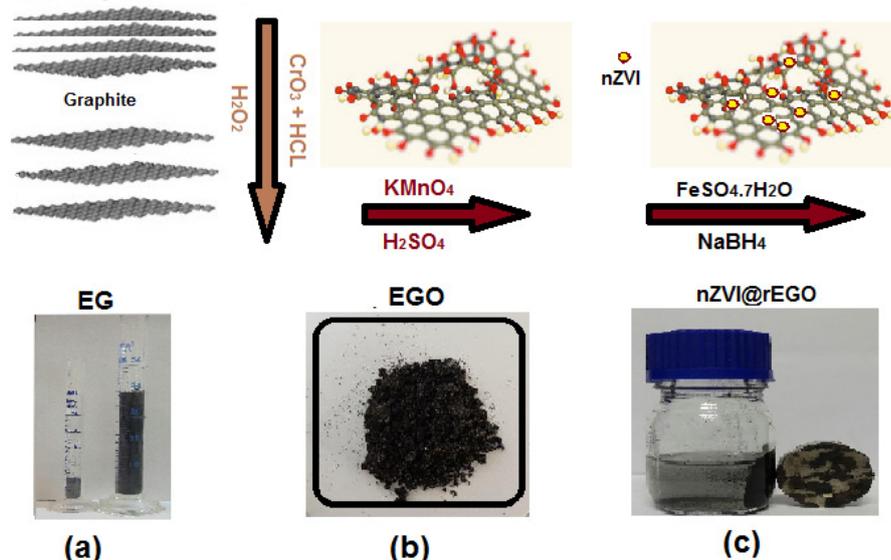
Figure 2. Preparation of (a) EG, (b) EGO, and (c) nZVI@rEGO

ice bath and it was leaved without mechanical mixing for 4 hours. Afterwards, the EG was added to the mixture and it was leaved for 2 hours to generate EGO. To complete the oxidation process, the produced EGO was soaked in diluted H_2O_2 solution and cooled in an ice bath. Then, the EGO was washed with distilled water and ethanol 4 consecutive times (32). Figure 2b shows the mechanism of oxidation process.

To predicate nZVI on EGO, Fan et al. method was used (33). For this purpose, 1 g of EGO was scattered in distilled water for 2 hours and 5 g of $FeSO_4·7H_2O$ was mixed in 50 mL of distilled water, then, it was added to the suspended EGO where mixing was continued for 12 hours. The reducing solution was prepared by dissolving 1.4 g of $NaBH_4$ as a reducing agent in 50 mL of distilled water. Then, it was slowly added to the previous mixture where Fe^{+2} was converted to nZVI according to Eq. (11) (39-41). Figure 2c shows the mechanism of nZVI@rEGO formation.

$$Fe^{2+} + 2BH_4^- + 6H_2O \rightarrow Fe^0 + 2B(OH)_3 + 7H_2 \uparrow \quad (11)$$
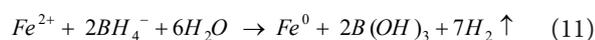
Characteristics and analytical methods

VEGA3/TESCAN-Libusina trida device was employed to provide the scanning electron microscope (SEM) and energy dispersive spectroscopy (EDS) analyses, which show the surface morphology and surface elemental composition of compounds.

X-ray diffraction (XRD) patterns of samples were recorded on an X-ray diffractometer (X'Pert PRO MPD, PANalytical Company) with a CuKa radiation source at 40 kV and 40 mA.

The MB concentration was measured by measuring the absorption of light at a maximum wavelength of 664 nm. For this purpose, first, different concentrations of dye were prepared. Then, their absorption was measured at a maximum wavelength of 664 nm using a DR 5000 spectrophotometer manufactured by HACH. Then, the calibration curve was obtained by plotting the amount of adsorption in terms of concentration. Finally, by placing the adsorption of the samples in the resulting line equation, the dye concentration was calculated (42). Heidolph MR Hei-Standard magnetic stirrer was also used for mixing the solution. Solution pH values were adjusted by 0.1 M HCl and NaOH solutions. A Metrohm 691 pH meter was used to measure the pH of solutions. To quench the reaction, Soubh et al method was applied (43).

Batch oxidation experiments

The batch method was employed to perform tests. Briefly, MB solution was placed in a glass flask, then, a certain amount of PS and nZVI@rEGO was added to the solution. Afterwards, the mixture was stirred at 80 rpm. Finally, the concentration of MB was determined at specified time intervals.

To choose the optimum operating conditions, the degradation tests were performed at different ranges of pH (3-9), nZVI@rEGO dose (0.4-1.6 g L^{-1}), PS concentration (0.192-0.768 g L^{-1}), contact time (0-60 minutes), and temperature (5-50°C). All experiments were conducted with 10 mg L^{-1} of MB. The removal efficiency of MB was estimated according to Eq. (12).

$$Removel\ (\%) = \left[(C_i - C_f)/\ C_f\right] \times 100 \quad (12)$$

Where C_i and C_f are the initial and final MB concentrations, respectively.

Results

Figures 3a and 3b show the XRD patterns of NFG and nZVI@rEGO, respectively. Figures 4a to 4b show the SEM images of NFG and nZVI@rEGO, respectively. In order to

investigate the effect of pH on the MB removal efficiency, different values of pH (3, 5, 7, and 9) were investigated, the results are presented in Figure 5. The effect of different nZVI@rEGO doses (0.4-1.6 g L^{-1}) with equal intervals of 0.4 g L^{-1} on the removal efficacy of MB was studied at MB concentration = 10 mg L^{-1}, PS concentration = 0.288 g L^{-1}, pH = 3, and reaction time = 25 min, the results are illustrated in Figure 6. The effect of different PS concentrations (0.192-0.768 g L^{-1}) on the removal efficiency of MB was studied at MB concentration = 10 mg L^{-1}, nZVI@rEGO dose = 1.2 g L^{-1}, pH = 3, and reaction time = 25 minutes, and the results are illustrated in Figure 7. In order to determine the optimal time of the nZVI@rEGO/PS process, the experiments were performed again under optimal conditions (MB concentration = 10 mg L^{-1}, nZVI@rEGO dose = 1.2 g L^{-1}, PS concentration = 0.576 g L^{-1}, pH = 3, and reaction time = 0-180 minutes), and the results are shown in Figure 8. The effect of temperature on the performance of nZVI@rEGO/PS and PS processes under optimal conditions (MB concentration = 10 mg L^{-1}, nZVI@rEGO dose = 1.2 g L^{-1}, PS concentration = 0.576 g L^{-1}, pH = 3, and reaction time = 20 minutes) was studied. For better understanding of the impact of temperature on the removal efficacy of MB by the nZVI@rEGO/PS process, the degradation rate constants were evaluated at temperature of 5, 25, and 50°C in the presence and absence of nZVI@rEGO.

Discussion

Characterization of NFG, EGO, and nZVI@rEGO

As shown in Figure 3a, the XRD patterns of NFG show an intense peak at 2θ angle of 26°. While it decreased significantly in the XRD patterns of EGO and nZVI@
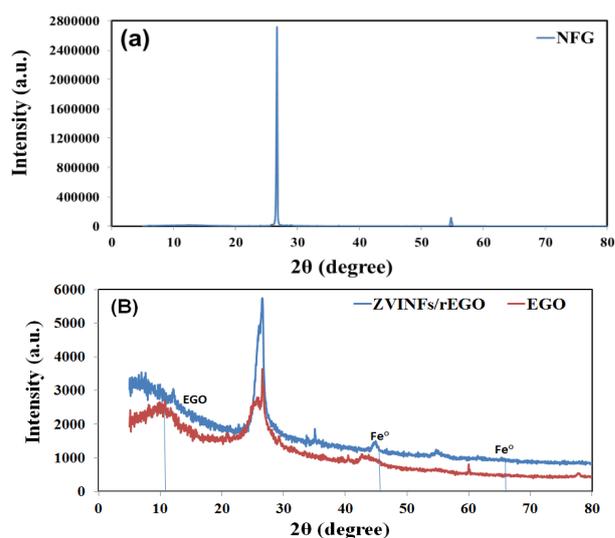
Figure 3. Powder XRD pattern of (a) NFG and (b) EGO and nZVI@rEGO.

rEGO (Figure 3b), this is due to the processes of expansion and oxidation (32). The XRD patterns of nZVI@rEGO confirm the presence of ZVI at 2θ angles of 44.7° and 65°, which is consistent with the results of previous studies (33,44).

The SEM images for NFG, EGO, and ZVINFs/rULGO are shown in Figures 4a to 3C, respectively. As shown in Figure 4b, the EGO surface became more suitable to carry nanoparticles where the nZVI is placed on the EGO surface in the chain structure with a diameter about 100 nm (Figure 4c). As shown in Figure 4f, EDS analyses of
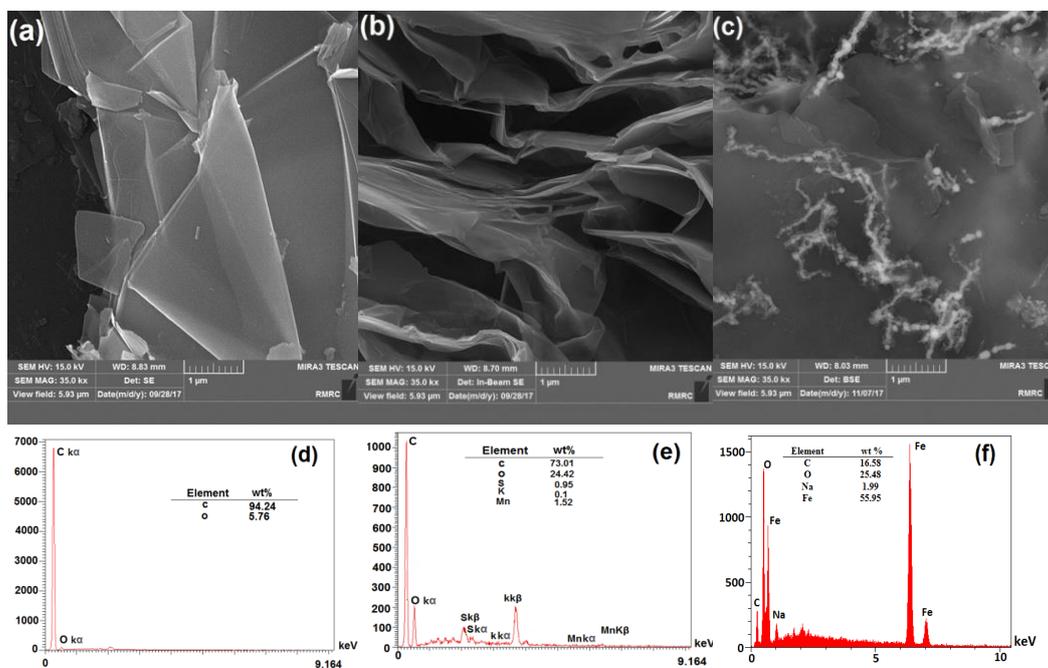
Figure 4. SEM images at 35 KX of (a) NFG, (b) EGO, and (c) nZVI@rEGO, (d) the corresponding EDS spectrum of (e) NFG, (e) EGO, and (f) nZVI@rEGO.
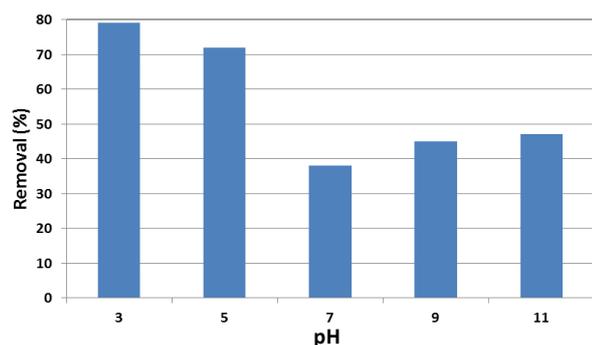
Figure 5. Effect of pH on the MB removal under experimental conditions: MB concentration = 10 mg L^{-1}, PS concentration = 0.288 g L^{-1}, nZVI@rEGO dose = 1.1 g L^{-1}, reaction time = 25 min.
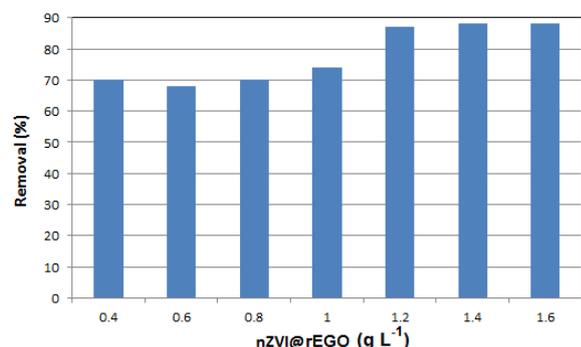
Figure 6. Effect of nZVI@rEGO dosage on the MB removal under experimental conditions: MB concentration = 10 mg L^{-1}, PS concentration = 0.288 g L^{-1}, pH = 3, reaction time = 25 min

nZVI@rEGO indicate the existence of Fe element with an amount greater than 50%, which increases the possibility of its use as a PS activator. The EDS analyses also show an increase in the proportion of oxygen from 5.76% in NFG (Figure 4d) to 24.42% in EGO (Figure 4e), indicating the success of the oxidation process of EG.

Effect of pH

The solution pH has a significant effect on the quantity and type of radicals formed in sulfate radical advanced oxidation processes (SR-AOPs) (45). In the nZVI@rEGO/PS process, pH has a significant effect on the decomposition of PS through its effect on dissolving nZVI (46). As shown in Figure 5, the removal efficiency of MB increased by decreasing the solution pH, and the maximum removal efficiency of MB was 79% at pH 3. That is because, at acidic conditions, nZVI is decomposed to Fe^{+2} according to Eq. (1). This led to an increase in activting PS according to Eq. (6).

By increasing pH, the removal efficacy of MB was decreased to a minimum value at pH 7. This is due to the formation of iron hydroxide and the reduced presence of iron ions in the solution, according to Eqs. (13-16) (47). By reaching pH to 9 and 11, the removal efficacy of MB increased slightly because alkaline conditions contribute

to the activation of PS (48,49).

$$Fe^{2+} + H_2O \rightarrow FeOH^+ + H^+ \tag{13}$$

$$Fe^{3+} + H_2O \rightarrow Fe(OH)^{2+} + H^+ \tag{14}$$

$$Fe^{3+} + 2H_2O \rightarrow Fe(OH)_2^+ + 2H^+ \tag{15}$$

$$2Fe^{3+} + 2H_2O \rightarrow Fe_2(OH)_2^{4+} + 2H^+ \tag{16}$$
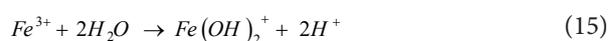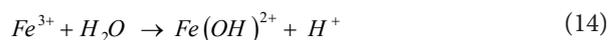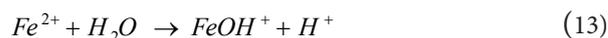
Maximum removal efficiency of anthraquinone dye reactive blue 19 (RB19) using PS/ZVI system has been reported at acidic conditions, i. e. pH 3 (50). In another study, the maximum degradation of nonylphenol by PS/nZVI-biochar was also reported at pH 3 (24). According to the results obtained from the experiments in this section, pH 3 can be considered as an optimal pH for the nZVI@rEGO/PS system.

Effect of nZVI@rEGO and PS dose

As illustrated in Figure 6, the increase of nZVI@rEGO dosage from 0.4 to 1.2 g L^{-1} increased the removal efficacy of MB from 70% to 87%. This can be due to the increased activation of PS, according to Eqs. (6), and as a result, increasing the dose of dissolved Fe^{2+} ions, according to Eqs.
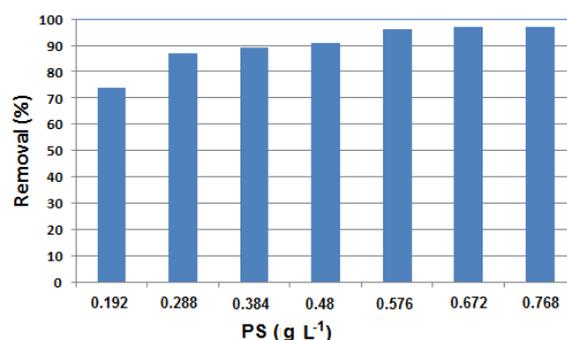
Figure 7. Effect of PS dose on the MB removal under experimental conditions: MB concentration = 10 mg L^{-1}, nZVI@rEGO dose = 1.2 g L^{-1}, pH = 3, reaction time = 25 min
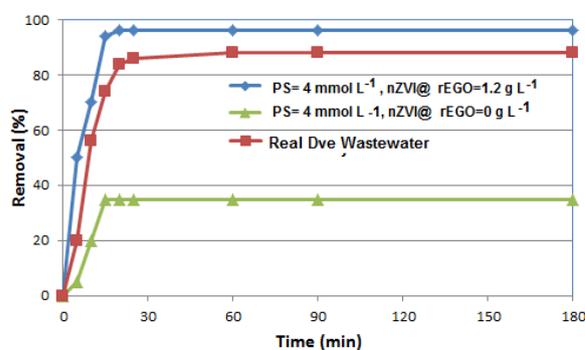
Figure 8. Effect of reaction time on the MB removal under optimal conditions: MB concentration = 10 mg L^{-1}, nZVI@rEGO dose = 1.2 g L^{-1}, PS concentration = 0.576 g L^{-1}, pH = 3, reaction time = 180 min.

(1-4). Subsequently, the increase over that dosage did not cause a significant improvement in the removal efficacy of MB. This is because the increasing of concentrations of dissolved Fe^{2+} ions can quench SR, according to Eq. (16) (51,52).

$$Fe^{2+} + SO_4^{\cdot-} \rightarrow SO_4^- + Fe^{3+} \qquad (16)$$
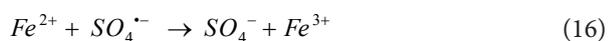
In other study, the increasing of ZVI dosage over 0.8 g L^{-1} did not significantly improve the decolorization rate of anthraquinone dye reactive blue 19 by the combination of PS and ZVI. Therefore, the nZVI@rEGO dosage of 1.2 g L^{-1} was chosen as the optimal dose for subsequent experiments.

In SR-AOPs, PS dose is one of the effective factors in removing the target contaminant (8). As illustrated in Figure 7, by increasing the PS dose from 0.192 to 0.576 g L^{-1}, the removal efficiency of MB increased from 74 to 96%. By increasing the PS dose higher than 0.576 g L^{-1}, there was no improvement in the removal efficacy of MB. That is because the increase of PS above a certain limit can quench SR, according to Eq. (17) (52). Also, sulfate radicals can react with each other, as a result, they have a quenching effect on the sulfate radical production at high concentration, according to Eq. (18) (15). Le et al have reported that an increase in the initial PS concentration above 20 mM had a negative effect on the removal rate of anthraquinone dye reactive blue 19 in the nZVI/PS system (50). Therefore, the PS dose of 0.576 g L^{-1} was selected to perform the following experiments.

$$SO_4^{\cdot-} + S_2O_8^{2-} \rightarrow S_2O_8^- + SO_4^{2-} \qquad (17)$$

$$SO_4^{\cdot-} + SO_4^{\cdot-} \rightarrow S_2O_8^{2-} \qquad (18)$$
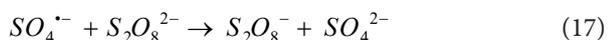
Effect of reaction time and temperature

As can be seen in Figure 8, at reaction time of 20 minutes, the removal efficiency of MB was 96%, after that the removal efficiency of MB remained almost constant. This can be explained by the fact that the role of divalent iron ions is much greater than trivalent iron in the activation of PS. In the first minutes of the experiment, due to the high concentration of divalent iron ions, the reaction rate was high, which over time and decreasing the concentration of this ion and its conversion to trivalent iron ions (Eq. 16) (36), the process of PS activation also decreased sharply, and as a result, leads to its poor performance. In a study by Hung et al, iron oxide was used as a PS activator to remove MB dye, and similar results were reported regarding the removal efficiency after the optimal time (1). Thus, the reaction time of 20 minutes was selected as the optimum reaction time. At optimum conditions, the removal efficiency of MB was 37% in the absence of activator. Because PS is hydrolyzed alone in the absence of activator, according to Eq. (19) (53).

$$S_2O_8^{2-} + 2H_2O \rightarrow 2HSO_4^- + H_2O_2 \qquad (19)$$
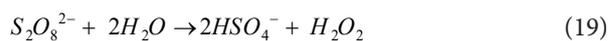
In order to investigate the removal mechanism, some experiments were conducted using PS, EGO, nZVI, and nZVI@rEGO/PS (Figure 9). For this purpose, the effect of PS and nZVI@rEGO on the removal of MB was tested separately, and the related removal efficiencies were significantly lower than that of the nZVI@rEGO/PS system. These results confirmed that the sulfate radical is the main component involving in the removal of MB. In addition, the low removal efficiency obtained using EGO is an indication of its low adsorption efficiency. As shown in Figure 9, only 18.7% removal of MB was observed in the ZVI process. The removal of MB occurred due to the ZVI surface adsorption and reduction.

As shown in Figure 10, by increasing temperature from 25 to 50°C, the removal efficiency of MB was increased from 35% to 51% by the PS process and from 96% to 98% by the nZVI@rEGO/PS process. As heat is considered as an activator of PS that increases removal efficiency, therefore, increasing temperature improved the removal efficiency (54). At temperature of 5°C, the removal efficiency of MB by the PS process decreased to 9%. While, there was no significant change in the removal efficiency of MB by the nZVI@rEGO/PS process. This feature makes nZVI@rEGO/PS process suitable to work at low temperatures.

Removal of MB from real dye wastewater

The impact of nZVI@rEGO/PS process on dye-containing wastewater was examined. For this purpose, a series of experiments were performed on the diluted real dye wastewater samples with MB (10 mg L^{-1}) under optimum conditions. Dye wastewater was obtained from pump station of a tannery wastewater treatment plant. As concentration of MB in the supplied wastewater was high, for providing comparable concentration of MB (10 mg/L), supplied wastewater was diluted by distilled water. The characteristics of diluted wastewater were: COD (98 mg L^{-1}) and Cl^- (440 mg L^{-1}). As shown in Figure 8, the removal efficiency of MB from real dye wastewater was
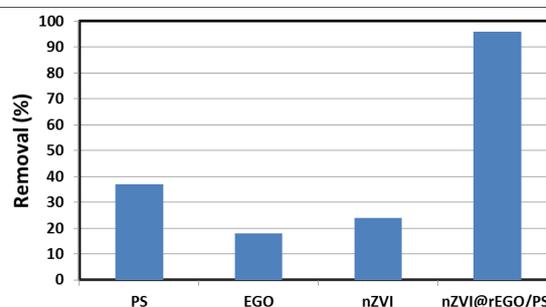
Figure 9. Comparative evaluation of different systems (PS, EGO, nZVI, and nZVI@rEGO/PS) under optimal conditions: MB concentration = 10 mg L^{-1}, nZVI@rEGO dose = 1.2 g L^{-1}, PS concentration = 0.576 g L^{-1}, pH = 3, reaction time = 180 min
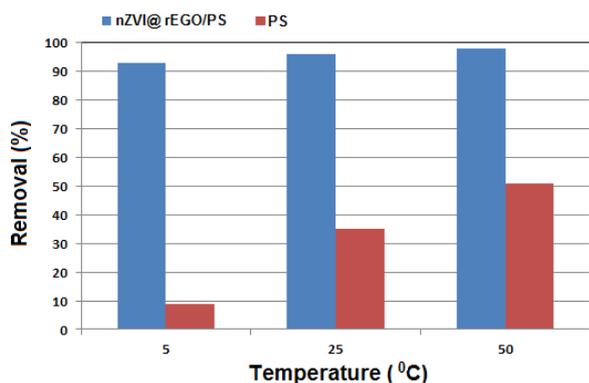
Figure 10. Effect of temperature on the MB removal under optimal conditions: MB concentration = 10 mg L^{-1}, nZVI@rEGO dose = 1.2 g L^{-1}, PS concentration = 0.576 g L^{-1}, pH = 3, reaction time = 20 min.

88%, while the removal efficiency of MB from synthetic wastewater was 96%. This decrease in removal efficiency can be explained by the fact that the real wastewater mainly contains a variety of organic and inorganic contaminants which could decrease contacts with MB (55,56), as well as chloride ion which can scavenge oxidant radicals, and as a result, leads to a decrease in the removal efficiency (57,58).

Identification of predominant radicals in nZVI@rEGO/PS process

To identify the dominant radical species in nZVI@rEGO/PS process, alcohols were used to quench the hydroxyl and sulfate radicals. Therefore, ethanol (alcohol with alpha hydrogen) as hydroxyl and sulfate radical scavenger and tert-butyl alcohol (TBA) with no alpha hydrogen were used as effective quenching agents for hydroxyl radicals (59). In this study, alcohol (EtOH, TBA) concentration used was 1 M. The results clearly showed that aniline degradation was significantly decreased by adding alcohols. As shown in Figure 11, aniline degradation in nZVI@rEGO/PS process without any radical scavenger was 96%. However, in the presence of ethanol (EtOH), only 18% MB removal was observed. While in the presence of TBA, the MB removal was 63%. The results revealed that the reaction was completely quenched by adding EtOH as $^{\cdot}$OH radical and $SO_4^{\cdot-}$ radical scavenger, while with the addition of TBA, the removal rate of MB was moderately influenced.

Kinetic modeling

Kinetics study indicated that nZVI@rEGO/PS decolorization is a pseudo-first-order reaction, which can be expressed according to Eq. (20) (50). As illustrated in Figures 10a and 10b, in the absence of nZVI@rEGO, the degradation rate constants of MB at temperatures of 5, 25, and 50°C were 2.5 × 10^{-3}, 19.5 × 10^{-3}, and 29.1 × 10^{-3} min^{-1}, respectively (Figure 12a). However, in the presence of nZVI@rEGO, the degradation rate constants of MB at temperatures of 5, 25, and 50°C were 96.4 × 10^{-3}, 135 ×

10^{-3}, and 150.3 × 10^{-3} min^{-1}, respectively (Figure 12b). In other words, the presence of nZVI@rEGO contributed to strengthening of the degradation rate constants, at above-mentioned temperatures. It has been reported that increasing ferrous concentration from 1 to 4 mM resulted in an increase in the degradation rate constant of Orange G from 0.04 to 0.12 min^{-1} in ferrous/persulfate system (60).

$$\ln(C_t / C_0) = -kt \tag{20}$$

The Arrhenius equation (Eq. 21) was used to evaluate the activation energy of reaction at above-mentioned temperatures (61).

$$lnk = lnA - E_a / RT \tag{21}$$

Where k is the pseudo first-order rate constant (min^{-1}), A is the pre-exponential factor (min^{-1}), E_a is the activation energy (kJ mol^{-1}), R is the universal gas constant (0.0083 kJ mol^{-1}), and T is the solution temperature (K). It could be observed that there is a strong linear relationship between lnk and 1/T (Figure 13), the presence of nZVI@rEGO decreased the activation energies of MB removal from 45.9 to 8.32 kJ mol^{-1} (Table 1). In other words, it caused 5.5 times decrease in E_a of MB removal. This decline in E_a is attributed to the activation provided by the nZVI@rEGO of PS. In other words, generation of SR at this level need less E_a, and as a result, the existence of nZVI@rEGO with PS together in the solution (62). In other studies, the activation energy was decreased from 120.4 to 36.1 kJ mol^{-1} using Fe^0 as an activator of PS for degradation of acetaminophen (15), and the activation energy was 98 kJ mol^{-1} using ZVI as an activator of PS for decolorization of anthraquinone dye reactive blue 19 (50).

Conclusion

This study investigated the removal efficiency of MB in aqueous solutions by the nZVI@rEGO/PS process. The
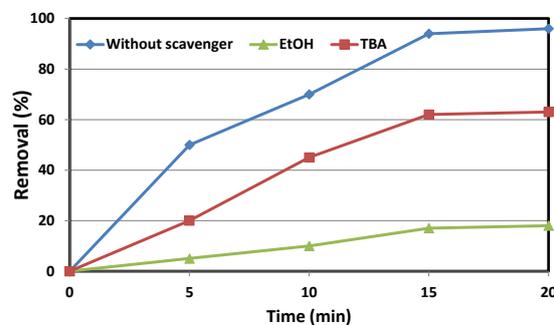
Figure 11. Effect of EtOH and TBA as radical scavengers on the MB removal under optimal conditions in the nZVI@rEGO/PS process: MB concentration = 10 mg L^{-1}, nZVI@rEGO dose = 1.2 g L^{-1}, PS concentration = 0.576 g L^{-1}, pH = 3, reaction time = 20 min
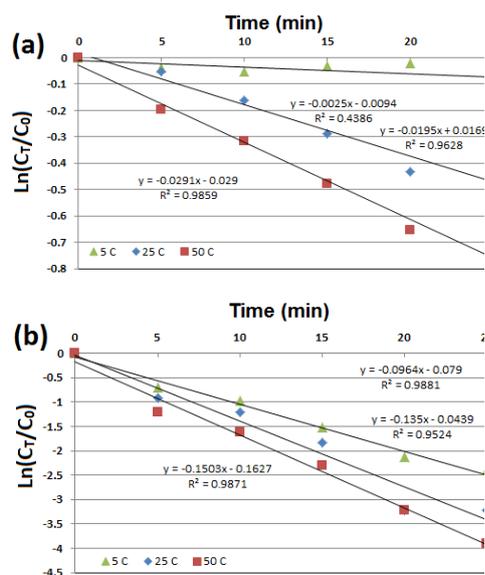
Figure 12. Effect of temperature on the removal rate of MB (a) in the absence of nZVI@rEGO and (b) in the presence of nZVI@rEGO, under optimal conditions: MB concentration = 10 mg L^{-1}, nZVI@rEGO dose = 1.2 g L^{-1}, PS concentration = 0.576 g L^{-1}, pH = 3, reaction time = 20 min

experiments proved the effectiveness of the use of nZVI@rEGO as an acivator of PS for removal of MB. EGO was proposed as an efficient bed for the immobilization of nZVI. EDS analysis of nZVI@rEGO indicates the existence of Fe element to an amount greater than 50%. The XRD patterns of nZVI@rEGO confirmed the presence of ZVI at the 2θ angles of 44.7° and 65°. The addition of 1.2 g L^{-1} of nZVI@rEGO at temperatures of 5, 25, and 50°C led to 38.56, 6.92, and 5.16 times, respectively, increase in degradation rate of MB. The presence of nZVI@rEGO decreased the activation energies of MB degradation from 45.9 to 8.3 kJ mol^{-1}. In other words, it caused 5.5 times decrease in E_a of MB removal.

Acknowledgments

Ethical issues

The authors certify that this this manuscript is the original work of the authors, all data collected during the study are presented in this manuscript, and no data from the study has been or will be published elsewhere separately.

Competing interests

The authors declare that they have no conflict of interests.

Author's contributions

The tests were conceived and prepared by AMS, and data analysis and writing of the manuscript were performed by all authors.
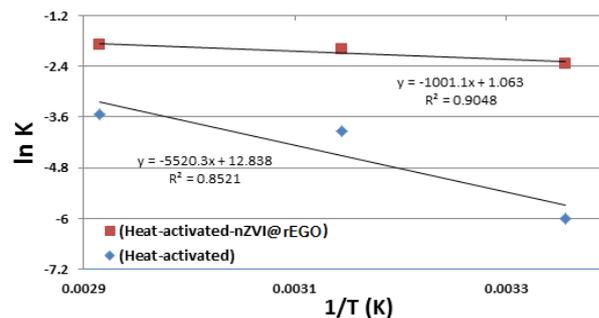
Figure 13. lnk$_{obs}$ versus T^{-1} for removal of MB by the PS and nZVI@rEGO/PS systems according to Arrhenius equation, under optimal conditions: MB concentration = 10 mg L^{-1}, nZVI@rEGO dose= 1.2 g L^{-1}, PS concentration = 0.576 g L^{-1}, pH = 3, reaction time = 20 min

Table 1. The parameters calculated at different temperatures

Temperature	nZVI@rEGO/PS			Heat-activated PS		
	298K	318K	343K	298K	318K	343K
K$_1$,.10^{-3} min^{-1}	29.7	1	4.4	96.4	135	150.3
R (kJ mol^{-1})	0.0083			0.0083		
Lnk=lnA-E$_a$/RT	Y=1001.1X+1.063			Y=5520.3X+12.838		
E$_a$ (kJ/mol^{-1})	8.32			45.9		
A (min^{-1})	2.89			376246.578		

References

1. Hung CM, Chen CW, Liu YY, Dong CD. Decolorization of methylene blue by persulfate activated with FeO magnetic particles. Water Environ Res 2016; 88(8): 675-86. doi: 10.2175/106143016x14609975746848.

2. Xiao X, Zhang F, Feng Z, Deng S, Wang Y. Adsorptive removal and kinetics of methylene blue from aqueous solution using NiO/MCM-41 composite. Physica E Low Dimens Syst Nanostruct 2015; 65: 4-12. doi: 10.1016/j.physe.2014.08.006.

3. Alene AN, Abate GY, Habte AT. Bioadsorption of basic blue dye from aqueous solution onto raw and modified waste ash as economical alternative bioadsorbent. J Chem 2020; 2020: 8746035. doi: 10.1155/2020/8746035.

4. Royer B, Cardoso NF, Lima EC, Vaghetti JC, Simon NM, Calvete T, et al. Applications of Brazilian pine-fruit shell in natural and carbonized forms as adsorbents to removal of methylene blue from aqueous solutions--kinetic and equilibrium study. J Hazard Mater 2009; 164(2-3): 1213-22. doi: 10.1016/j.jhazmat.2008.09.028.

5. Ding F, Xie Y, Peng W, Peng YK. Measuring the bioactivity and molecular conformation of typically globular proteins with phenothiazine-derived methylene blue in solid and in solution: a comparative study using photochemistry and computational chemistry. J Photochem Photobiol B 2016; 158: 69-80. doi: 10.1016/j.jphotobiol.2016.02.029.

6. Zawadzki P. Decolorisation of methylene blue with sodium persulfate activated with visible light in the presence of glucose and sucrose. Water Air Soil Pollut 2019; 230(12): 313. doi: 10.1007/s11270-019-4372-x.

7. Zhen G, Lu X, Zhao Y, Chai X, Niu D. Enhanced dewaterability of sewage sludge in the presence of Fe(II)-

activated persulfate oxidation. Bioresour Technol 2012; 116: 259-65. doi: 10.1016/j.biortech.2012.01.170.

8. Abu Amr SS, Aziz HA, Adlan MN, Bashir MJ. Pretreatment of stabilized leachate using ozone/persulfate oxidation process. Chem Eng J 2013; 221: 492-9. doi: 10.1016/j.cej.2013.02.038.

9. Soubh A, Mokhtarani N. The post treatment of composting leachate with a combination of ozone and persulfate oxidation processes. RSC Adv 2016; 6(80): 76113-22. doi: 10.1039/c6ra09539a.

10. Anipsitakis GP, Dionysiou DD, Gonzalez MA. Cobalt-mediated activation of peroxymonosulfate and sulfate radical attack on phenolic compounds. implications of chloride ions. Environ Sci Technol 2006; 40(3): 1000-7. doi: 10.1021/es050634b.

11. Soubh AM. Assessment of steel slag as a persulfate activator for treatment of landfill leachate. Open Access Journal of Waste Management & Xenobiotics 2019; 2(3): 1-6. doi: 10.23880/oajwx-16000125.

12. Soubh AM, Baghdadi M, Abdoli MA, Aminzadeh B. Zero-valent iron nanofibers (ZVINFs) immobilized on the surface of reduced ultra-large graphene oxide (rULGO) as a persulfate activator for treatment of landfill leachate. J Environ Chem Eng 2018; 6(5): 6568-79. doi: 10.1016/j.jece.2018.10.011.

13. Graça CA, Fugita LT, de Velosa AC, Teixeira A. Amicarbazone degradation promoted by ZVI-activated persulfate: study of relevant variables for practical application. Environ Sci Pollut Res Int 2018; 25(6): 5474-83. doi: 10.1007/s11356-017-0862-9.

14. Meserghani M, Nikaeen M, Jonidi Jafari A, Dehghani MH, Bina B. Amoxicillin degradation with electro-persulfate combined with H2O2 from aqueous solution using response surface methodology. Environ Health Eng Manag 2020; 7(3): 209-16. doi: 10.34172/ehem.2020.24.

15. Deng J, Shao Y, Gao N, Deng Y, Tan C, Zhou S. Zero-valent iron/persulfate(Fe0/PS) oxidation acetaminophen in water. Int J Environ Sci Technol 2014; 11(4): 881-90. doi: 10.1007/s13762-013-0284-2.

16. Zhao J, Zhang Y, Quan X, Chen S. Enhanced oxidation of 4-chlorophenol using sulfate radicals generated from zero-valent iron and peroxydisulfate at ambient temperature. Sep Purif Technol 2010; 71(3): 302-7. doi: 10.1016/j.seppur.2009.12.010.

17. Crane RA, Scott TB. Nanoscale zero-valent iron: Future prospects for an emerging water treatment technology. J Hazard Mater 2012; 211-212: 112-25. doi: 10.1016/j.jhazmat.2011.11.073.

18. Shih YH, Tai YT. Reaction of decabrominated diphenyl ether by zerovalent iron nanoparticles. Chemosphere 2010; 78(10): 1200-6. doi: 10.1016/j.chemosphere.2009.12.061.

19. Zhan J, Zheng T, Piringer G, Day C, McPherson GL, Lu Y, et al. Transport characteristics of nanoscale functional zerovalent iron/silica composites for in situ remediation of trichloroethylene. Environ Sci Technol 2008; 42(23): 8871-6. doi: 10.1021/es800387p.

20. Phenrat T, Saleh N, Sirk K, Tilton RD, Lowry GV. Aggregation and sedimentation of aqueous nanoscale zerovalent iron dispersions. Environ Sci Technol 2007; 41(1): 284-90. doi: 10.1021/es061349a.

21. Pasinszki T, Krebsz M. Synthesis and application of zero-valent iron nanoparticles in water treatment, environmental remediation, catalysis, and their biological effects. Nanomaterials (Basel) 2020; 10(5):917. doi: 10.3390/nano10050917.

22. Li A, Tai C, Zhao Z, Wang Y, Zhang Q, Jiang G, et al. Debromination of decabrominated diphenyl ether by resin-bound iron nanoparticles. Environ Sci Technol 2007; 41(19): 6841-6. doi: 10.1021/es070769c.

23. Zhang X, Lin S, Chen Z, Megharaj M, Naidu R. Kaolinite-supported nanoscale zero-valent iron for removal of Pb2+ from aqueous solution: reactivity, characterization and mechanism. Water Res 2011; 45(11): 3481-8. doi: 10.1016/j.watres.2011.04.010.

24. Hussain I, Li M, Zhang Y, Li Y, Huang S, Du X, et al. Insights into the mechanism of persulfate activation with nZVI/BC nanocomposite for the degradation of nonylphenol. Chem Eng J 2017; 311: 163-72. doi: 10.1016/j.cej.2016.11.085.

25. Zhu BW, Lim TT, Feng J. Reductive dechlorination of 1,2,4-trichlorobenzene with palladized nanoscale Fe(zero-valent) particles supported on chitosan and silica. Chemosphere 2006; 65(7): 1137-45. doi: 10.1016/j.chemosphere.2006.04.012.

26. Wang Y, Sun H, Duan X, Ang HM, Tadé MO, Wang S. A new magnetic nano zero-valent iron encapsulated in carbon spheres for oxidative degradation of phenol. Appl Catal B Environ 2015; 172-173: 73-81. doi: 10.1016/j.apcatb.2015.02.016.

27. Jabeen H, Chandra V, Jung S, Lee JW, Kim KS, Kim SB. Enhanced Cr(vi) removal using iron nanoparticle decorated graphene. Nanoscale 2011; 3(9): 3583-5. doi: 10.1039/c1nr10549c.

28. Adlnasab L, Djafarzadeh N, Maghsodi A. A new magnetic bio-sorbent for arsenate removal from the contaminated water: characterization, isotherms, and kinetics. Environ Health Eng Manag 2020; 7(1): 49-58. doi: 10.34172/ehem.2020.07.

29. Wang J, Chen B, Xing B. Wrinkles and folds of activated graphene nanosheets as fast and efficient adsorptive sites for hydrophobic organic contaminants. Environ Sci Technol 2016; 50(7): 3798-808. doi: 10.1021/acs.est.5b04865.

30. Wang J, Chen B. Adsorption and coadsorption of organic pollutants and a heavy metal by graphene oxide and reduced graphene materials. Chem Eng J 2015; 281: 379-88. doi: 10.1016/j.cej.2015.06.102.

31. Pu S, Deng D, Wang K, Wang M, Zhang Y, Shangguan L, et al. Optimizing the removal of nitrate from aqueous solutions via reduced graphite oxide-supported nZVI: synthesis, characterization, kinetics, and reduction mechanism. Environ Sci Pollut Res Int 2019; 26(4): 3932-45. doi: 10.1007/s11356-018-3813-1.

32. Dong L, Chen Z, Lin S, Wang K, Ma C, Lu H. Reactivity-controlled preparation of ultralarge graphene oxide by chemical expansion of graphite. Chem Mater 2017; 29(2): 564-72. doi: 10.1021/acs.chemmater.6b03748.

33. Fan M, Li T, Hu J, Cao R, Wu Q, Wei X, et al. Synthesis and characterization of reduced graphene oxide-supported nanoscale zero-valent iron (nZVI/rGO) composites used for Pb(II) removal. Materials (Basel) 2016; 9(8):687. doi: 10.3390/ma9080687.

34. Wang C, Luo H, Zhang Z, Wu Y, Zhang J, Chen S. Removal of As(III) and As(V) from aqueous solutions

using nanoscale zero valent iron-reduced graphite oxide modified composites. J Hazard Mater 2014; 268: 124-31. doi: 10.1016/j.jhazmat.2014.01.009.

35. Li J, Chen C, Zhu K, Wang X. Nanoscale zero-valent iron particles modified on reduced graphene oxides using a plasma technique for Cd(II) removal. J Taiwan Inst Chem Eng 2016; 59: 389-94. doi: 10.1016/j.jtice.2015.09.010.

36. Ahmad A, Gu X, Li L, Lv S, Xu Y, Guo X. Efficient degradation of trichloroethylene in water using persulfate activated by reduced graphene oxide-iron nanocomposite. Environ Sci Pollut Res Int 2015; 22(22): 17876-85. doi: 10.1007/s11356-015-5034-1.

37. Mittal J, Konno H, Inagaki M. Synthesis of graphite intercalation compounds with CrVI compounds using CrO3 and HCl at room temperature. Synth Met 1998; 96(2): 103-8. doi: 10.1016/S0379-6779(98)00070-8.

38. Skowroński JM. Exfoliation of graphite-CrO3 intercalation compounds in hydrogen peroxide solution. J Mater Sci 1988; 23(6): 2243-6. doi: 10.1007/bf01115794.

39. Li Y, Zhang Y, Li J, Zheng X. Enhanced removal of pentachlorophenol by a novel composite: nanoscale zero valent iron immobilized on organobentonite. Environ Pollut 2011; 159(12): 3744-9. doi: 10.1016/j.envpol.2011.07.016.

40. Prema P, Selvarani M. Inactivation of bacteria using chemically fabricated zerovalent iron nanoparticles. Int Res J Pharm Sci 2012; 3(1): 27-31.

41. Selvarani M, Prema P. Removal of toxic metal hexavalent chromium [cr(vi)] from aqueous solution using starch–stabilized nanoscale zerovalent iron as adsorbent: equilibrium and kinetics. Int J Environ Sci 2012; 2(4): 1962-75. doi: 10.6088/ijes.00202030080.

42. Zhao L, Yang S, Wang L, Shi C, Huo M, Li Y. Rapid and simple spectrophotometric determination of persulfate in water by microwave assisted decolorization of Methylene Blue. J Environ Sci 2015; 31: 235-9. doi: 10.1016/j.jes.2014.09.036.

43. Soubh AM, Baghdadi M, Abdoli MA, Aminzadeh B. Activation of persulfate using an industrial iron-rich sludge as an efficient nanocatalyst for landfill leachate treatment. Catalysts 2018; 8(5): 218. doi: 10.3390/catal8050218.

44. Hoch LB, Mack EJ, Hydutsky BW, Hershman JM, Skluzacek JM, Mallouk TE. Carbothermal synthesis of carbon-supported nanoscale zero-valent iron particles for the remediation of hexavalent chromium. Environ Sci Technol 2008; 42(7): 2600-5. doi: 10.1021/es702589u.

45. Mokhtarani N, Khodabakhshi S, Ayati B. Optimization of photocatalytic post-treatment of composting leachate using UV/TiO2. Desalin Water Treat 2016; 57(47): 22232-43. doi: 10.1080/19443994.2015.1130652.

46. Ahmad A, Gu X, Li L, Lu S, Xu Y, Guo X. Effects of pH and anions on the generation of reactive oxygen species (ROS) in nZVI-rGo-activated persulfate system. Water Air Soil Pollut 2015; 226(11): 369. doi: 10.1007/s11270-015-2635-8.

47. Govindan K, Raja M, Maheshwari SU, Noel M. Analysis and understanding of amido black 10B dye degradation in aqueous solution by electrocoagulation with the conventional oxidants peroxomonosulfate, peroxodisulfate and hydrogen peroxide. Environ Sci Water Res Technol 2015; 1(1): 108-19. doi: 10.1039/c4ew00030g.

48. Furman OS, Teel AL, Watts RJ. Mechanism of base

49. Liang C, Guo YY. Remediation of diesel-contaminated soils using persulfate under alkaline condition. Water Air Soil Pollut 2012; 223(7): 4605-14. doi: 10.1007/s11270-012-1221-6.

50. Le C, Wu JH, Li P, Wang X, Zhu NW, Wu PX, et al. Decolorization of anthraquinone dye Reactive Blue 19 by the combination of persulfate and zero-valent iron. Water Sci Technol 2011; 64(3): 754-9. doi: 10.2166/wst.2011.708.

51. Monteagudo JM, Durán A, González R, Expósito AJ. In situ chemical oxidation of carbamazepine solutions using persulfate simultaneously activated by heat energy, UV light, Fe2+ ions, and H2O2. Appl Catal B Environ 2015; 176-177: 120-9. doi: 10.1016/j.apcatb.2015.03.055.

52. Yang S, Yang X, Shao X, Niu R, Wang L. Activated carbon catalyzed persulfate oxidation of Azo dye acid orange 7 at ambient temperature. J Hazard Mater 2011; 186(1): 659-66. doi: 10.1016/j.jhazmat.2010.11.057.

53. House DA. Kinetics and mechanism of oxidations by peroxydisulfate. Chem Rev 1962; 62(3): 185-203. doi: 10.1021/cr60217a001.

54. Liang C, Wang ZS, Bruell CJ. Influence of pH on persulfate oxidation of TCE at ambient temperatures. Chemosphere 2007; 66(1): 106-13. doi: 10.1016/j.chemosphere.2006.05.026.

55. Moussavi G, Mahdavianpour M. The selective direct oxidation of ammonium in the contaminated water to nitrogen gas using the chemical-less VUV photochemical continuous-flow reactor. Chem Eng J 2016; 295: 57-63. doi: 10.1016/j.cej.2016.03.035.

56. Dutta K, Mukhopadhyay S, Bhattacharjee S, Chaudhuri B. Chemical oxidation of methylene blue using a Fenton-like reaction. J Hazard Mater 2001; 84(1): 57-71. doi: 10.1016/s0304-3894(01)00202-3.

57. Liao CH, Kang SF, Wu FA. Hydroxyl radical scavenging role of chloride and bicarbonate ions in the H2O2/UV process. Chemosphere 2001; 44(5): 1193-200. doi: 10.1016/s0045-6535(00)00278-2.

58. Mahdavianpour M, Ildari S, Ebrahimi M, Moslemzadeh M. Decolorization and mineralization of methylene blue in aqueous solutions by persulfate/Fe2+ process. J Water Chem Technol 2020; 42(4): 244-51. doi: 10.3103/S1063455X20040098.

59. Hussain I, Zhang Y, Huang S. Degradation of aniline with zero-valent iron as an activator of persulfate in aqueous solution. RSC Adv 2014; 4(7): 3502-11. doi: 10.1039/c3ra43364a.

60. Xu XR, Li XZ. Degradation of azo dye Orange G in aqueous solutions by persulfate with ferrous ion. Sep Purif Technol 2010; 72(1): 105-11. doi: 10.1016/j.seppur.2010.01.012.

61. Hasan M, Ahmad AL, Hameed BH. Adsorption of reactive dye onto cross-linked chitosan/oil palm ash composite beads. Chem Eng J 2008; 136(2-3): 164-72. doi: 10.1016/j.cej.2007.03.038.

62. Oh SY, Kim HW, Park JM, Park HS, Yoon C. Oxidation of polyvinyl alcohol by persulfate activated with heat, Fe2+, and zero-valent iron. J Hazard Mater 2009; 168(1): 346-51. doi: 10.1016/j.jhazmat.2009.02.065.

activation of persulfate. Environ Sci Technol 2010; 44(16): 6423-8. doi: 10.1021/es1013714.